PERGAMON

International Journal of Solids and Structures 39 (2002) 225–249

INTERNATIONAL JOURNAL OF SOLIDS and STRUCTURES

www.elsevier.com/locate/ijsolstr

An explicit formulation of a three-dimensional material damping model with transverse isotropy

M. Dalenbring

Aeronautics Division, FFA, FOI, Swedish Defence Research Agency, P.O. Box 11021, S-161 11 Bromma, Sweden

Received 25 April 2000

Abstract

A constitutive three-dimensional (3D) damping model is derived for transversely isotropic material symmetry, using the augmented Hooke's law [Intl. J. Solids Struct. 32 (1995) 2835] as a starting point. The proposed material model is tested numerically, via finite-element techniques, on a laminate structure built from stacked aluminium and Plexiglas plates. Effective 3D transversely isotropic material properties are given in terms of homogeneous material damping functions in connection with homogenised elastic laminate properties. Comparisons made between the results from the elastic (undamped) eigenvalue problem of the detailed (layerwise) model of the laminate and the effective 3D elastic model show that the homogenised model is reasonably accurate, in terms of predicted elastic eigenfrequencies for the first 20 modes. The dynamic homogenisation process, with damping included, is evaluated in terms of forced vibration response for the laminate structure, using effective transversely isotropic frequency dependent material properties. The dynamic 3D effective homogeneous material model is found to simulate very closely the detailed model in the studied frequency interval for the numerical test case.

Keywords: Constitutive material damping modelling; Linear viscoelasticity; Transverse isotropy; Homogeneous materials; Laminate structures; Finite element displacement modes; Modal analysis; Structural vibrations

1. Introduction

Combinations of different materials in the form of composite structures are commonly used in many engineering applications, especially in the aerospace and automotive industries. One of the major benefits of using composites, compared to standard metallic materials, is the high strength-to-weight ratio, resulting in a low structural weight. The passive damping in traditional composite structures is higher than in standard metallic materials but still quite low. In the field of vibro-acoustics, development of new combinations of standard composites and highly damped materials of viscoelastic type are currently receiving increasing attention in order to control structural vibrations and find cost efficient designs. For this purpose,

E-mail address: dgm@foi.se (M. Dalenbring).

0020-7683/01/$ - see front matter
PII: S0020-7683(01)00158-5

numerical models and optimisation techniques are needed to predict the dynamic behaviour of general (anisotropic) composite structures and minimise the amount of experimental testing needed. Refined theoretical models often result in increase of size and complexity of the model and the chosen solution method is then often a trade off between details and maximum allowable model size. In this context, it is highly attractive to use effective (macro-mechanical) models, defined as a homogeneous and generally anisotropic representative volume of the composite structure with the interaction between structural details included at a less refined constitutive level, in order to reduce the model size. Another desired feature in development and use of different material models is the possibility and simplicity of extraction of material damping parameters from vibration damping, observed in dynamic testing of assembled structures, such as layered plates and composite structures.

The main objective of the present work is to derive a general (three-dimensional (3D)) constitutive formulation, including damping, in case of transversely isotropic material symmetry, for vibro-acoustic simulation of damped structural vibrations. This material symmetry is valid for stacked isotropic materials and a selected class of composite laminates with quasi-isotropic behaviour. A full (state-of-the-art) treatment of various aspects of damping modelling in composite structures are today available in the form of many references and modern text books (e.g. Chandra et al., 1999; Gibson, 1990, 1994; Finegan and Gibson, 1999; Sun and Lu, 1995). However, most applications are based on two-dimensional plate and shell models. To the authors knowledge there are very few works published on 3D modelling of damped composite plates, which also was confirmed in the review paper by Chandra et al. (1999).

The field of damping modelling of composite structures may be divided into two approaches. Methods of the first type are based on the elastic–viscoelastic correspondence principle (Hashin, 1970; Christensen, 1979; Sun and Lu, 1995). In the literature, a number of advanced (viscoelastic) constitutive material models have been proposed by Bagley and Torvik (1983), Lesieutre and Bianchini (1995), Barbero and Luciano (1995) and Dovstam (1995), as the use of a simple constant damping loss factor model is inconsistent (non-causal) and inadequate for highly damped real materials. A review on material damping and alternative (linear) constitutive models, and a unified approach in the field of vibration modelling, may be found in the recent paper by Dovstam (2000a).

The second type of models for modelling of damping in built-up structures is based on the so-called strain energy method, introduced by Unger and Kerwin (1962). The loss factor is determined as the ratio between the dissipation in the material to the energy stored in the material. The total damping (losses) in a composite structure may then be given as a sum of the damping in each constituent element. In practice, the strain energy method is evaluated in terms of modal strain energies at each resonance of the structure (cf. Johnson and Kienholz, 1982; Hwang and Gibson, 1991; Saravanos and Chamis, 1991; Barrett, 1992; Rikards et al., 1993, 1994; Saravanos, 1994; Saravanos and Pereira, 1995; Koo and Lee, 1995; Yarlagadda and Lesieutre, 1995; Korjakin et al., 1998; Maher et al., 1999a,b). In the case of general geometry and boundary conditions the strain energies are conveniently computed by using finite-element (FE) approximations. Modern theories often use higher-order deformation theories, to account for the transverse shear and rotational inertia effects, as the classical plate theory is found to be inadequate in applications to thick-section laminates. Another important aspect is the existence of coupling in laminates due to geometry, orientation, stacking sequence, constituent layer properties and the vibration mode of interest. Topics such as coupling and 3D effects (interlaminar stresses) on damping of laminates have been investigated by Hwang and Gibson (1991, 1992a,b) and Hwang et al. (1992) by performing 3D analyses based on the strain energy method and layerwise FE analysis on typical laminate structures. Further, there exists another type of modal coupling, present also in homogeneous structures, due to the damping itself, pointed out by Dovstam (1997). The last effect may be taken care of by using an unconditionally convergent modal approach, proposed by Dovstam (1998, 2000b), and adopted in the proposed paper. This modelling technique provides a clear separation of pure elastic behaviour and (anelastic) damping behaviour.

The 3D constitutive stress–strain relationship is based on linear irreversible thermodynamics and expressed in the form of a generally anisotropic augmented Hooke's law (Dovstam, 1995). The augmented Hooke's law (AHL) was explicitly formulated for the case of isotropic materials in terms of two material damping functions (Dovstam, 1995). The technique was successfully applied to simulate vibrations of real isotropic materials (Dalenbring, 2001a), and found to be particularly suitable for developing a general experimental material damping estimation procedure (Dovstam and Dalenbring, 1997; Dalenbring, 1999).

In order to estimate material damping parameters (anelastic), the elastic (static) material parameters of the structure need to be known. Methods for extraction of elastic material parameters of laminates are usually based on two-dimensional plate and shell theories in connection with higher-order deformation theory (cf. Reddy and Phan, 1985) and recently Khdeir and Reddy (1999), Carrera (2000) and Kant and Swaminathan (2000). Alternative, 3D, effective anisotropic material models start with Postma (1955) and Rytov (1956), in the field of geophysics, proposing effective solutions for wave propagation in infinite periodically layered medium of two isotropic materials. Methods for extracting 3D elastic (static) material parameters for layered media most often rely on the long wavelength assumption concerning the state of stress and strain in each lamina, in connection with a constitutive model of the equivalent homogeneous material. Each laminate is further assumed to be approximately infinite in extent or built from a very large number of repeated layers, with each lamina thickness small compared to the global dimensions. The effective elastic material moduli for general orthotropic material symmetry may then be given in a closed-form "rule of mixture" as geometrically weighted averages of the constituent parts of the laminate structure, cf. Christensen (1979). Similar methods, for extraction of 3D effective elastic material moduli, have been developed by Chou and Carleone (1972), Pagano (1974), Sun and Li (1988) and recently by Chen and Tsai (1996) and Whitcomb and Noh (2000), by using the (first-order) approximation that interlaminar shear stresses are constant through the laminate. Pagano (1969, 1970) showed that transverse stresses calculated by using the classical laminated plate theory and invoking equilibrium considerations converge to the exact solution (within the framework of linear theory of elasticity) when the thickness-aspect-ratio increases, i.e., if the plate is sufficiently thin compared to other dimensions. The approach developed by Sun and Li (1988) have been shown to be efficient and accurate both in terms of static and dynamic (undamped) analysis of thick-section laminates by Sun et al. (1996). Roy and Tsai (1992) used exact solutions for three boundary value problems to extract 3D effective homogenised material parameters. This procedure was used to study the accuracy of different methods, for numerical extraction of 3D effective moduli, with respect to the number of layers, thickness and stacking sequence, with special interest in the interlaminar direction. Roy and Tsai (1992) conclude that the effective parameter estimation methods, referenced by them, give accurate results for laminates built from more than 20 layers.

The main contributions of the present paper are: formulation of a new explicit constitutive damping model for transversely isotropic material symmetry, with five corresponding material damping functions (Section 2), and implementation of the new damping model in a refined unconditionally convergent modal response model (Section 3), suitable for damping estimation.

The ability of the proposed material model is numerically tested on a typical thin laminate structure, comprised of two aluminium plates and one Plexiglas plate, by comparing the response of the effective (homogenised) FE model with the response of a corresponding detailed (layerwise) FE model. Effective 3D (homogenised) elastic properties of the test structure are approximated by the method proposed by Chen and Tsai (1996), for determination of effective transverse laminate properties, in connection with use of the classical laminated plate theory for in-plane properties (cf. Sun and Li, 1988; Hyer, 1998). The method adopted here for approximation of effective elastic material parameters is one possible choice; any accurate 3D method that correctly accounts for the deformation in the laminate structure may thus be used.

2. Material damping model

A 3D, completely general, constitutive material model for small strain applications was proposed by Dovstam (1995), with explicit expressions for the model parameters derived for the case of isotropic material damping. The particular case of transversely isotropic material symmetry is considered here with the plane of isotropy defined as the 1–2 plane (Fig. 1; (cf. Reddy, 1997)). This implies no restriction in the sense that a transversely isotropic material may always be arbitrarily oriented with material moduli obtained by appropriate transformations (or cyclic permutations). Matrices and variables not explicitly defined in the text are defined in Appendices A and B. Following Dovstam, continuous material properties are then formally given in the Laplace domain ($s = \mathrm{i}2\pi f$ and f is the current frequency of vibration) by an augmented Hooke's law:

$$\mathbf{T} = \hat{\mathbf{H}}(\mathbf{x}, s)\mathbf{E}, \tag{1}$$

$$\hat{\mathbf{H}}(\mathbf{x}, s) = \mathbf{H}(\mathbf{x}) + \mathbf{H}_{\Delta}(\mathbf{x}, s), \tag{2}$$

where $\mathbf{H}_{\Delta}(\mathbf{x}, s)$ defines the damping and the matrix $\mathbf{H}(\mathbf{x})$, with components H_{ij}, denotes a generalised elastic Hooke's matrix and $\mathbf{T}$ and $\mathbf{E}$ the standard stress and engineering strain vectors respectively. The elasticities of the material studied here may be defined by the five independent measurable engineering constants E_1, v_{21}, E_3, v_{31} and G_{31}. Two of these five constitutive parameters correspond to in-plane (1)–(2) stresses and strains. For transverse material isotropy, the material constants are defined by Young's modulus E_1 (here $E_2 = E_1$ from isotropy) and the Poisson's ratio v_{21} (here $v_{12} = v_{21}$ from isotropy) or, alternatively, the shear modulus $G_{12} = E_1/(2(1 + v_{21}))$. The remaining out-of-plane material parameters are related to the transverse stress and strain with the corresponding engineering constants given by the elastic transverse moduli E_3, Poisson's ratio v_{31} ($v_{31} = v_{32}$) and the shear modulus G_{31} ($G_{31} = G_{23}$). The five independent elastic material Hooke's matrix components H_{ij}, $i, j = 1, 2, \ldots, 6$, expressed in terms of engineering constants (cf. Christensen, 1979), are given by:

$$\mathbf{H} = H_{11}\mathbf{H}_{11} + H_{12}\mathbf{H}_{12} + H_{13}\mathbf{H}_{13} + H_{33}\mathbf{H}_{33} + H_{66}\mathbf{H}_{66}, \tag{3}$$

$$H_{11} = G_{12} + \kappa_{21}, \tag{4}$$

$$H_{12} = -G_{12} + \kappa_{21}, \tag{5}$$

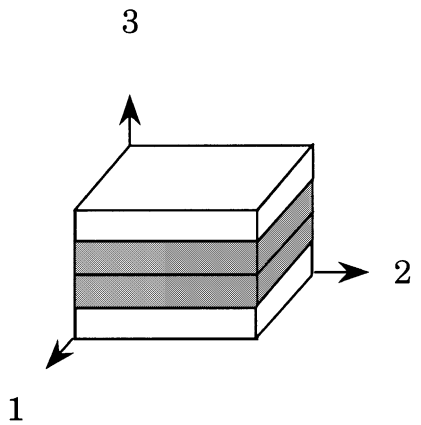

Fig. 1. A typical representative volume element of the [aluminium/Plexiglas]$_s$ test laminate structure.

$$H_{13} = 2\nu_{31}\kappa_{21}, \tag{6}$$

$$H_{33} = E_3 + 4\nu_{31}^2\kappa_{21}, \tag{7}$$

$$H_{66} = G_{31}, \tag{8}$$

$$\kappa_{21} = \frac{E_1}{4(1-\nu_{31}^2 E_1/E_3) - E_1/G_{12}}, \tag{9}$$

where κ_{21} corresponds to the in-plane (1)–(2) elastic engineering bulk modulus.

The material damping, defined by the augmentation $\mathbf{H}_{\Delta}(\mathbf{x},s)$ in Eq. (2), is generated by a linear combination of five independent, augmented Hooke's material moduli, using coupling matrices $\mathbf{F}_l$, with corresponding material damping parameters a_l, b_l, c_l, d_l and e_l, defined in Appendix B. After some simple but tedious algebraic manipulations it is possible to relate the augmentation $\mathbf{H}_{\Delta}(\mathbf{x},s)$ in Eq. (2) to the constant matrices $\mathbf{H}_{ik}$ in Eq. (3) as:

$$\mathbf{H}_{\Delta} = d_{11}(s)H_{11}\mathbf{H}_{11} + d_{12}(s)H_{12}\mathbf{H}_{12} + d_{13}(s)H_{13}\mathbf{H}_{13} + d_{33}(s)H_{33}\mathbf{H}_{33} + d_{66}(s)H_{66}\mathbf{H}_{66}, \tag{10}$$

where the five material damping functions, $d_{11}(s)$, $d_{12}(s)$, $d_{13}(s)$, $d_{33}(s)$ and $d_{66}(s)$, are given as the sums:

$$d_{11}(s) = \sum_{l=1}^{N_a} \frac{A_{11}^{(l)} s}{(\beta_l + s)}, \quad \left\{A_{11}^{(l)} \geqslant 0\right\} \in \mathbf{R}, \tag{11}$$

$$d_{12}(s) = \sum_{l=1}^{N_a} \frac{A_{12}^{(l)} s}{(\beta_l + s)}, \quad \left\{A_{12}^{(l)} \leqslant (H_{11}/H_{12})A_{11}^{(l)}\right\} \in \mathbf{R}, \tag{12}$$

$$d_{13}(s) = \sum_{l=1}^{N_a} \frac{A_{13}^{(l)} s}{(\beta_l + s)}, \quad A_{13}^{(l)} \in \mathbf{R}, \tag{13}$$

$$d_{33}(s) = \sum_{l=1}^{N_a} \frac{A_{33}^{(l)} s}{(\beta_l + s)}, \quad \left\{A_{33}^{(l)} \geqslant 0\right\} \in \mathbf{R}, \tag{14}$$

$$d_{66}(s) = \sum_{l=1}^{N_a} \frac{A_{66}^{(l)} s}{(\beta_l + s)}, \quad \left\{A_{66}^{(l)} \geqslant 0\right\} \in \mathbf{R} \tag{15}$$

and $A_{11}^{(l)}$, $A_{12}^{(l)}$, $A_{13}^{(l)}$, $A_{33}^{(l)}$ and $A_{66}^{(l)}$ are "process amplitudes" with corresponding real positive relaxation frequencies β_l, $l = 1, 2, 3, \ldots, N_a$, and accordingly relaxation times $\tau_l = 1/\beta_l$. The damping functions $d_{12}(s)$ and $d_{13}(s)$, corresponding to the off-diagonal terms of the material matrix, may be negative but the process amplitudes must be real (cf. Dovstam, 1995). Note here also (cf. Eq. (12)), that the amplitude $A_{12}^{(l)}$ depends on H_{11}, H_{12} and $A_{11}^{(l)}$.

The complex, frequency dependent, engineering moduli of the damped material are expressed in terms of the AHL parameters as:

$$\hat{E}_1(s) = \frac{2(H_{11}(1+d_{11}(s)) + H_{12}(1+d_{12}(s)))}{\left[\frac{H_{33}(1+d_{33}(s))}{\hat{E}_3(s)} + \frac{(H_{11}(1+d_{11}(s))+H_{12}(1+d_{12}(s)))}{(H_{11}(1+d_{11}(s))-H_{12}(1+d_{12}(s)))}\right]}, \tag{16}$$

$$\hat{\nu}_{21}(s) = \frac{\hat{E}_1(s)}{H_{11}(1+d_{11}(s)) - H_{12}(1+d_{12}(s))} - 1, \tag{17}$$

$$\hat{E}_3(s) = H_{33}(1 + d_{33}(s)) - \frac{2H_{13}^2(1 + d_{13}(s))^2}{H_{11}(1 + d_{11}(s)) + H_{12}(1 + d_{12}(s))}, \tag{18}$$

$$\hat{v}_{31}(s) = \frac{H_{13}(1 + d_{13}(s))}{H_{11}(1 + d_{11}(s)) + H_{12}(1 + d_{12}(s))}, \tag{19}$$

$$\hat{G}_{31}(s) = H_{66}(1 + d_{66}(s)). \tag{20}$$

Here the elastic (static) material parameters are frequency independent. The frequency dependence of the material parameters is defined by the five damping functions $d_{11}(s)$, $d_{12}(s)$, $d_{13}(s)$, $d_{33}(s)$ and $d_{66}(s)$ in Eqs. (11)–(15).

3. Modal vibration response model

Modal models have been shown to be particularly useful in material damping estimation (Dovstam and Dalenbring, 1997; Dalenbring, 1999). The 3D modal vibration model introduced by Dovstam (1998, 2000b), is applicable for general continuously distributed material damping and boundary traction excitation. It is explicitly shown below how modal damping may be defined, for the particular case of a transversely isotropic material, as a linear combination of five damping functions and associated modal weight factors.

Following Dovstam, the 3D displacement field $\mathbf{u} = \mathbf{u}(\mathbf{x}, t)$ is expanded (in the Laplace domain) in terms of a generalised Fourier series:

$$\tilde{\mathbf{u}}(\mathbf{x}, s) = \sum_{m=1}^{\infty} c_m(\tilde{\mathbf{u}})\mathbf{w}^{(m)}(\mathbf{x}), \tag{21}$$

where $\{\mathbf{w}^{(m)}(\mathbf{x})\}_{m=1}^{\infty}$ constitutes a complete basis for 3D vector fields with locally (over the body) square intergrable component fields. The real, 3D, elastic, displacement modes $\mathbf{w}^{(m)}(\mathbf{x})$ and corresponding eigenfrequencies ω_m, are defined as solutions to the corresponding continuous elastic eigenvalue problem, defined by the generalised Hooke's material matrix $\mathbf{H}$ in Eq. (2), homogeneous boundary conditions and the geometry and mass distribution of the studied body. In applications the modes $\mathbf{w}^{(m)}(\mathbf{x})$ may be approximated by FE techniques.

Under the assumption of small modal coupling the Fourier coefficient spectra $c_m(\tilde{\mathbf{u}})$, $m = 1, 2, 3, \ldots$, may be approximated as Dovstam (1998, 2000b) (cf. Appendix B for the case of generally coupled modes):

$$c_m(\tilde{\mathbf{u}}) \approx \frac{\tilde{\boldsymbol{F}}_{\partial}^{(m)}(s)}{a_m\left(s^2 + \omega_m^2/(1 + \delta_m(s))\right)} = \frac{\tilde{F}_k(\mathbf{x}_e, s)w_k^{(m)}(\mathbf{x}_e)}{a_m\left(s^2 + \omega_m^2/(1 + \delta_m(s))\right)}, \tag{22}$$

where $a_m = 1$ if mass normalised displacement modes are used. The modal force spectrum $\tilde{\boldsymbol{F}}_{\partial}^{(m)}(s)$ is defined by the inner product (evaluated on the boundary) between the traction field and the modal displacement $\mathbf{w}^{(m)}(\mathbf{x})$. In the case of a local force excitation in the k direction at point $\mathbf{x}_e$ on the boundary, the modal force spectrum $\tilde{\boldsymbol{F}}_{\partial}^{(m)}(s)$ is determined by the force spectrum component $\tilde{F}_k(\mathbf{x}_e, s)$ multiplied by the elastic modal displacement component $w_k^{(m)}(\mathbf{x}_e)$.

The modal shift functions $\delta_m(s)$, $m = 1, 2, 3, \ldots$, in Eq. (22):

$$\delta_m(s) = \chi_{11}^{(m)}b(s) + \chi_{12}^{(m)}d(s) + \chi_{13}^{(m)}c(s) + \chi_{33}^{(m)}a(s) + \chi_{66}^{(m)}e(s), \tag{23}$$

are completely determined by the proposed set of material damping functions, defined below in Eqs. (24)–(28), and modal weight factors $\chi_{ij}^{(m)}$. The weight factors $\chi_{ij}^{(m)}$ equal the fraction of the modal elastic strain

energy corresponding to each independent (non-zero) modulus H_{ik} in Eq. (2) (cf. also Dovstam, 1997, 2000b), and may be approximated with good accuracy by post-processing discrete, undamped normal modes computed using standard FE techniques.

The transversely isotropic material functions in Eq. (23), corresponding to Eqs. (4)–(9) and Eqs. (B.1)–(B.8), are derived as:

$$a(s) = \frac{(E_3 - \hat{E}_3(s))}{\hat{E}_3(s)} + \frac{4\nu_{31}\kappa_{21}(\nu_{31} - 2\hat{\nu}_{31}(s))}{\hat{E}_3(s)} + \frac{8\nu_{31}^2\kappa_{21}^2(1 - \hat{\nu}_{21}(s))}{\hat{E}_1(s)(E_3 + 4\nu_{31}^2\kappa_{21})}, \tag{24}$$

$$b(s) = \frac{4\nu_{31}\kappa_{21}^2(\nu_{31} - 2\hat{\nu}_{31}(s))}{\hat{E}_3(s)(\kappa_{21} + G_{12})} + \frac{2\kappa_{21}^2(1 - \hat{\nu}_{21}(s))}{\hat{E}_1(s)(\kappa_{21} + G_{12})} + \frac{2G_{12}^2(1 + \hat{\nu}_{21}(s))}{\hat{E}_1(s)(\kappa_{21} + G_{12})} - 1, \tag{25}$$

$$c(s) = \frac{(E_3 + 4\nu_{31}^2\kappa_{21})(\nu_{31} - \hat{\nu}_{31}(s))}{\nu_{31}\hat{E}_3(s)} - \frac{4\nu_{31}\kappa_{21}\hat{\nu}_{31}(s)}{\hat{E}_3(s)} + \frac{2\kappa_{21}(1 - \hat{\nu}_{21}(s))}{\hat{E}_1(s)} - 1, \tag{26}$$

$$d(s) = \frac{4\nu_{31}\kappa_{21}^2(\nu_{31} - 2\hat{\nu}_{31}(s))}{\hat{E}_3(s)(\kappa_{21} - G_{12})} + \frac{2\kappa_{21}^2(1 - \hat{\nu}_{21}(s))}{\hat{E}_1(s)(\kappa_{21} - G_{12})} - \frac{2G_{12}^2(1 + \hat{\nu}_{21}(s))}{\hat{E}_1(s)(\kappa_{21} - G_{12})} - 1, \tag{27}$$

$$e(s) = \frac{(G_{31} - \hat{G}_{31}(s))}{\hat{G}_{31}(s)}, \tag{28}$$

with the complex frequency dependent engineering material moduli explicitly defined by Eqs. (16)–(20). It is important to note here that the modal shift function $\delta_m(s)$ is a structural property, Eq. (23), depending on both geometry and material parameters. Note also that the structural modal shift functions, $\delta_m(s) = 0$, $m = 1, 2, 3, \ldots$, are all zero if $s = 0$ (zero frequency) or alternatively if $\{a(s), b(s), c(s), d(s), e(s)\} = 0$ with $s \neq 0$. For zero/vanishing damping the resulting response model (Eqs. (21) and (22)) corresponds to the elastic (undamped) problem.

4. Numerical test example

4.1. The aluminium–Plexiglas test laminate structure

A simple numerical model of a realistic laminate structure was constructed in order to evaluate the proposed transversely isotropic material model for the homogenised medium. This material symmetry is relevant for symmetric laminates built from isotropic materials, and therefore chosen in the present paper. The test laminate structure was built by symmetric stacking of aluminium and Plexiglas plates, $[\text{Al}/\text{PMMA}]_s$, with nominal elastic (static) data for each material given in Table 1. The geometry of the four-layer aluminium–Plexiglas laminate, with nominal dimensions 520 mm × 300 mm × 6 mm and a thickness of each aluminium and Plexiglas layer of 1.5 mm, is shown in Fig. 2.

Table 1
Measured[a] elastic data for Plexiglas and aluminium

$E_{\text{Al}} = 73\,000$ MPa	$\nu_{\text{Al}} = 0.326$	$\rho_{\text{Al}} = 2795$ kg/m^3
$E_{\text{PMMA}} = 3440$ MPa	$\nu_{\text{PMMA}} = 0.382$	$\rho_{\text{PMMA}} = 1181$ kg/m^3

[a] At room temperature.

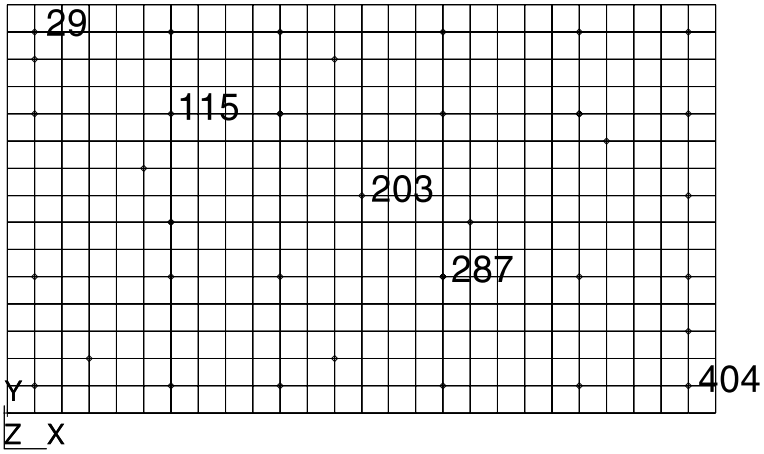

Fig. 2. Laminate geometry and FE boundaries. Evaluation points marked by numbers.

The dynamic system is characterised in terms of forced vibration responses, computed for different locations on the plate according to Fig. 4, with the excitation defined as a harmonic local force excitation (normal to the surface) and the boundaries taken as stress-free. The type of frequency responses discussed in the following will be receptances (cf. Ewins, 1986) defined as quotient spectra between vibration displacements (at the response points) and the force excitation.

4.2. Effective three-dimensional elastic laminate properties

The test structure is used to investigate the ability to establish a dynamic model of a typical laminate structure by defining a representative laminate volume element (Fig. 1) with effective (homogeneous) 3D constitutive behaviour, a first approximation to macro-mechanics (Hashin, 1970). This model of the test laminate structure is valid as long as local effects in the different layers may be neglected. The vibration frequency interval where the effective model results in high macroscopic accuracy generally varies from case to case, depending on geometry, orientation, stacking sequence and material properties. The vibration frequency interval may alternatively be stated in terms of corresponding vibrational wavelengths.

In the following, it is described how the effective 3D elastic material parameters may be calculated from known elasticities of the constituents of the test structure, given by nominal values in Table 2. For further details see Appendix C. From the discussion in Section 1 it is evident that the effective (homogenised) 3D homogeneous *elastic* properties, based on classical laminated plate theory and first-order shear deformation theory (for transverse properties), are accurate in the case of thin laminates. A layered plate may be defined "thin" if the local span-to-thickness ratio is greater than 20, according to Reddy (1997). The aluminium/Plexiglas test laminate structure have a thickness aspect ratio of approximately 50 and may thus be considered as thin. 3D, elastic effective transverse laminate properties are here approximated according to Chen and Tsai (1996) (Appendix C). Effective in-plane laminate properties are approximated by using the

Table 2
Calculated effective engineering transversely isotropic material constants for the symmetric homogenised aluminium–Plexiglas laminate

$E_{11} = 64307$ MPa	$\nu_{21} = 0.329$	$\rho = 1992$ kg/m^3
$E_{33} = 11398$ MPa	$G_{31} = 2381$ MPa	$\nu_{31} = 0.066$

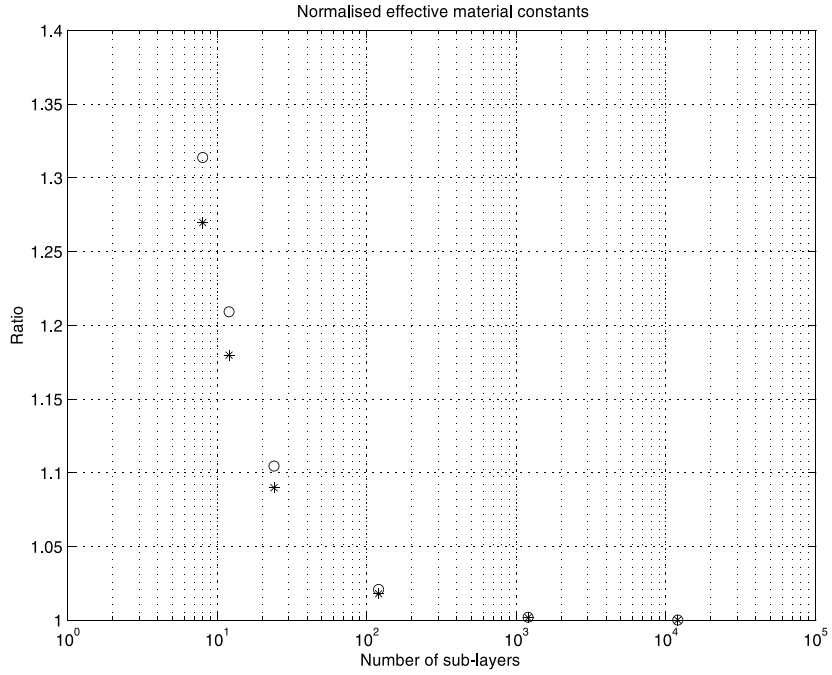

Fig. 3. Normalised effective in-plane material parameters, H_{11} ($\circ\circ\circ\circ$) and H_{12} ($*****$), using the classical laminated plate theory (normalised with respect to the results from the 3D method proposed by Chen and Tsai (1996)).

classical laminated plate theory (cf. Ernie and Rizzo, 1970; Hyer, 1998), in order to account for the bending effect in the laminate. Note here, according to Fig. 3, that the classical laminated plate theory gives the same result, in terms of effective in-plane elasticity properties, as the method proposed by Chen and Tsai (1996) when the number of laminae are large. The effective engineering constants are restricted to cases where the actual state of deformation in the composite material closely resemble the deformation assumptions made in the process of extraction of effective elastic parameters. A thorough investigation of assumptions made and the effect of boundaries is out of the scope of the present paper (cf. Pipes and Pagano, 1970; Reddy, 1997).

It is important to stress again that the focus in this paper is on the combined viscoelastic material model, based on the augmented Hooke's law, presented in Section 2. The first-order approximation method adopted here for extracting effective elastic material data is one possible choice. Alternative accurate (3D) techniques, which account for the deformation in each lamina, may also be used.

4.3. Effective elastic modal data for the aluminium–plexiglas laminate

The FE model of the laminate structure comprised a total of 390 isoparametric 20-node volume elements for the connected Plexiglas and aluminium layers, with four elements through the thickness. This FE model is sufficiently accurate for our purpose, with respect to discretisation errors, checked by performing a convergence test based on grid refinements. Possible shear locking was avoided by using proper element thickness-aspect-ratios (cf. Reddy, 1997). The plate geometry and element mesh is shown in Fig. 2. Modal data, in the form of 70 eigenvalues with corresponding eigenvectors and modal weight factors, were computed in ASKA Acoustics, Göransson (1988), with eigenfrequency $f_{70} = 5590$ Hz. A set of eigenfrequencies

Table 3
FE modal data for the effective homogenised aluminium–plexiglas laminate

Mode number (m)	Eigen frequency[a] (Hz)	Eigen frequency[b] (Hz)	Relative difference[c] (%)	Eigen frequency 3D (Hz)	Relative difference[c] (%)
7	129.9	131.7	1.4	130.0	0.1
8	135.5	136.0	0.4	135.9	0.3
9	303.5	306.3	0.9	305.0	0.5
10	355.3	361.1	1.6	356.5	0.3
11	401.4	411.3	2.5	402.8	0.3
12	488.4	500.2	2.4	491.1	0.6
13	541.1	549.4	1.5	544.9	0.7
14	669.1	680.7	1.7	674.3	0.8
15	727.9	749.8	3.0	733.9	0.8
16	869.7	886.4	2.0	877.2	1.0
17	970.4	991.8	2.2	981.7	1.2
18	1087.5	1123.4	3.3	1098.6	1.0
19	1132.8	1163.1	2.6	1145.2	1.1
20	1155.4	1193.2	3.2	1169.2	1.2

[a] Corresponding to the detailed FE model.
[b] Corresponding to classical laminated plate theory.
[c] With respect to the detailed model.

was here chosen as a measure of the modelling accuracy as a change in stiffness most often will give a more significant change in eigenfrequencies than in the corresponding mode shapes (cf. Maher, 1994; Chang, 1986; Carrera, 2000; Einarsson and Dalenbring, 2000).

The first 20 eigenfrequencies of the detailed (layerwise) FE model are compared with corresponding eigenfrequencies using classical laminated plate theory (standard isoparametric eight-node plate elements) and the proposed effective 3D anisotropic model (cf. Table 2). The result is presented in Table 3 together with the relative eigenfrequency error for each mode compared to the detailed model. The effective 3D material model is reasonably accurate, with a relative eigenfrequency difference of less than 1.2%, for the first 20 modes. The wavelength of mode number 20 is approximately 200 mm for the test laminate structure and consequently much larger than the laminate thickness (6 mm). There is an almost linear increase of the relative eigenfrequency difference between the detailed FE-model and the effective model, for the first 20 modes. The effective 3D model starts to deviate at higher modes, where the deformations in the constituents of the composite structure are different from those assumed in the homogenisation process.

The result from comparing eigenfrequencies, using the classical laminated plate theory and the corresponding detailed (layerwise) 3D FE model, show that the relative eigenfrequency difference (cf. Table 3) do not increase, with increasing mode number, in the same smooth way as when using the effective 3D model. The maximum relative eigenfrequency difference is also a factor two times larger than for the effective 3D model. The laminated plate theory may be improved by using higher-order interpolation of the displacement field, e.g., higher-order deformation plate theories (Reddy and Phan, 1985). A higher-order interpolation of the displacement field, in the 3D case, may be simulated by increase of the number of elements.

The modal weight factors, given by values in Table 4, corresponding to the modal strain energy associated with each independent, non-zero, elastic modulus, are essential in the definition of the modal response model in Section 3. The modal weight factors corresponding to the off diagonal terms in the material elasticity matrices (Eqs. (A.6)–(A.10)) may become negative, which is the case for this particular laminate structure, cf. Table 4. The sum of all five modal weight factors should for each mode be equal to one. The dominant part of the elastic modal strain energy, for this particular structure, is associated with the modal weight factor $\chi_{11}^{(m)}$, for the first 20 modes (cf. Table 4).

Table 4
Modal weight factors for the effective homogenised model

Mode number (m)	Modal weight factor				
	χ_{11}	χ_{12}	χ_{13}	χ_{33}	χ_{66}
7	1.2786	−0.2556	−0.0562	0.0281	0.0051
8	1.5041	−0.5270	−0.0046	0.0023	0.0252
9	1.4187	−0.4426	−0.0191	0.0095	0.0334
10	1.2662	−0.2581	−0.0543	0.0271	0.0191
11	1.1090	−0.0805	−0.0871	0.0435	0.0151
12	1.1436	−0.1363	−0.0753	0.0376	0.0304
13	1.3231	−0.3493	−0.0350	0.0175	0.0438
14	1.2970	−0.3240	−0.0393	0.0196	0.0467
15	1.0571	−0.0567	−0.0883	0.0441	0.0439
16	1.2562	−0.2925	−0.0438	0.0218	0.0583
17	1.2473	−0.2964	−0.0419	0.0208	0.0701
18	1.0277	−0.0354	−0.0912	0.0454	0.0534
19	1.1505	−0.1796	−0.0640	0.0319	0.0613
20	1.0505	−0.0738	−0.0829	0.0413	0.0649

4.4. Effective material model for the aluminium–Plexiglas laminate with damping

3D material damping may be introduced in the laminate structure according to Sections 2 and 3. First, detailed direct FE calculations were performed by layerwise modelling, with constituent properties for each separate isotropic material layer specified as given in Tables 1 and 5. Material damping was assigned only to the Plexiglas part of the laminate structure, i.e., the aluminium part was treated as having negligible damping. The material damping used for the Plexiglas part (cf. Dalenbring, 1999) is here "partly artificial", by modification of the process amplitudes (Table 6) to give a higher structural damping.

Secondly, the damped homogenised structure was defined as below. Effective damping parameter amplitudes were chosen by trial and error. This was done by repeated simulations with respect to changes in damping properties and minimising the difference between the vibration response of the homogenised 3D model and the corresponding detailed (layerwise) 3D FE model of the test laminate structure. The effective material was assumed to have the same damping process relaxation frequencies β_l as the Plexiglas material (cf. Tables 5 and 6). In addition, it was observed in this iterative process that a major part of the strain energy is associated with the modal weight factors $\chi_{11}^{(m)}$. It is important to stress that homogeneous material damping parameters cannot be calculated from knowledge of the damping of the parts by means provided in this paper. The homogeneous damping has to be defined as a constitutive property. The effective material parameter values used here are given in Tables 2 and 6, and the damping function $d_{11}(s)$ is plotted in Fig. 4.

Table 5
AHL damping parameters for Plexiglas[a]

AHL process number (l)	Relaxation frequency ($\beta_l/2\pi$)	Process amplitude	
		$(A_G^{(l)})$	$(A_\lambda^{(l)})$
1	1.59×10^{-1}	2.23×10	0
2	2.26×10	2.21×10	0
3	8.21×10	3.27	0
4	3.14×10^{2}	1.00×10^{-2}	0
5	3.84×10^{2}	1.32×10	0

[a] With modified process amplitudes.

Table 6
AHL damping parameters[a] for the homogenised model

AHL process number (l)	Relaxation frequency ($\beta_l/2\pi$)	Process amplitude	
		$(A_{11}^{(l)})$	$(A_{66}^{(l)})$
1	1.59×10^{-1}	8.00×10^{-2}	6.00×10
2	2.26×10	1.20×10^{-1}	0
3	8.21×10	0	0
4	3.14×10^{2}	0	0
5	3.84×10^{2}	5.80×10^{-2}	0

[a] With process amplitudes $A_{12}^{(l)}$, $A_{13}^{(l)}$ and $A_{33}^{(l)}$ are all zero.

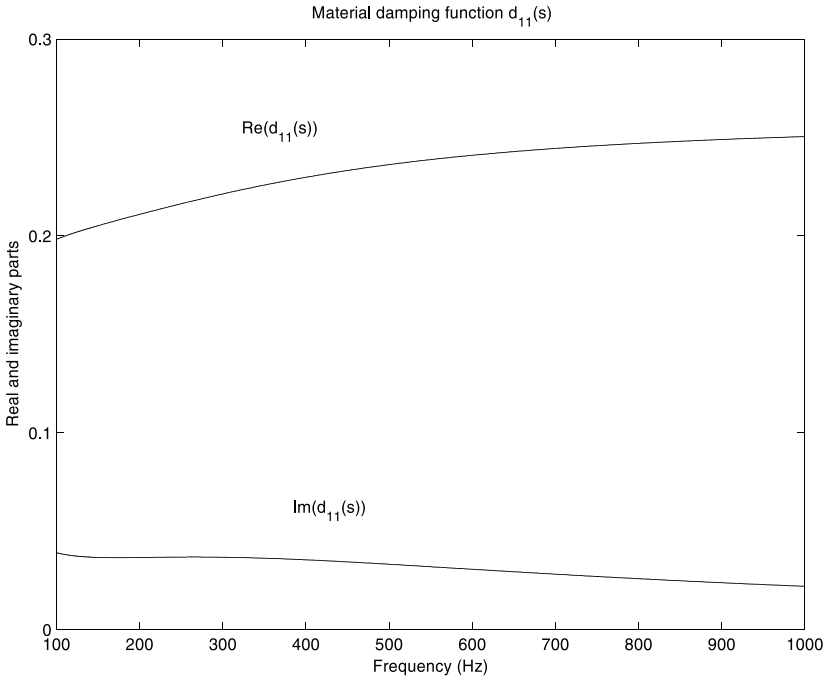

Fig. 4. Effective material damping function $d_{11}(s)$ (Eqs. (10) and (11)) for the structure. The real (upper curve) and imaginary (lower curve) parts of the anelastic part of the homogenised dynamic modulus are shown.

The damping function is presented for frequencies in the interval 100–1000 Hz, which includes the first 17 undamped eigenfrequencies of the structure (cf. Table 3). It is interesting to note that it is possible to simulate the structural damping of the homogenised transversely isotropic material sufficiently accurate by using only the material damping function, $d_{11}(s)$, (cf. Fig. 4) in Eq. (10). A general experimental estimation procedure for effective (homogenised) damping parameters, in analogy with the method proposed by Dovstam and Dalenbring (1997) and Dalenbring (1999), will be addressed in a forthcoming paper by Dalenbring (2001b).

The accuracy of the effective (homogenised) 3D vibration model is assessed by comparison with the corresponding detailed (layerwise) 3D FE model. The result from forced vibration response simulations, using the detailed finite-element model and the corresponding effective 3D (transversely isotropic and homogenised) generally coupled modal response model, at a selected number of points on the test structure is shown in Figs. 5–9. The agreement between the detailed FE model and the effective modal response

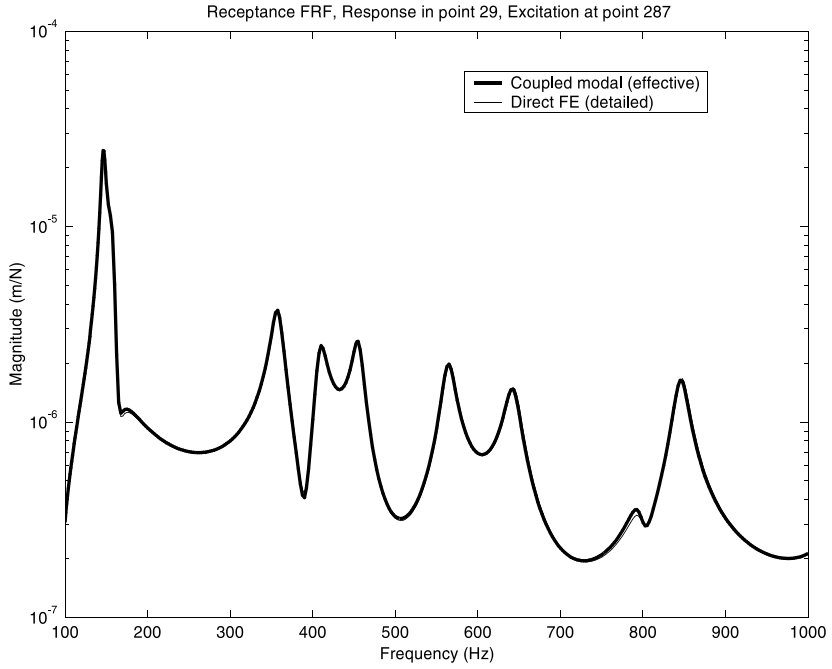

Fig. 5. Typical direct FE calculated (thin solid curve) transfer receptance FRF (response R_{33} in z-direction at point 29 and excitation in z-direction at point 287) for the laminate plate (with detailed modelling of the constituents) and corresponding effective coupled modal response model (thick solid curve), in the frequency interval 100–1000 Hz.

model is generally very good, in the studied frequency interval 100–1000 Hz. The models are compared in terms of vibration response amplitudes and damped resonance frequencies, corresponding to peaks in the curves in Figs. 5–9. A slight difference, for increasing frequency of vibration, may be seen in Fig. 8. This difference is probably due the details of the laminate structure, not accounted for in the effective model, at higher frequencies.

Finally, the accuracy of the two homogenised (3D) modal models is investigated by comparisons with the corresponding fully 3D homogenised FE model of test laminate structure. For comparison, also the response from the detailed (layerwise) model is plotted in the same graph. Figs. 10–15 show that the coupled modal model is in general very close to the result from the effective (homogeneous) FE model and the detailed model. The uncoupled modal model (computationally efficient and thus suitable for damping estimation) is found to be very accurate, except for response point number 115 (Fig. 11) in the frequency range 450–550 Hz, which is close to an anti-resonance (Fig. 6). The effect of truncation in the modal models, generally visible at frequencies close to an anti-resonance, is assumed to be limited due to the good agreement between the detailed (non-modal) model and the corresponding coupled modal model. The validity of the uncoupled modal model must be tested from case to case. The complex moduli used in the numerical simulation are strictly valid only in the frequency range of estimation and the accuracy generally varies from case to case, depending on geometry, stacking sequence and material properties.

5. Summary and conclusions

A 3D constitutive model is proposed for the case of transversely isotropic material symmetry. The constitutive model is based on the augmented Hooke's law, with the material damping described in terms of

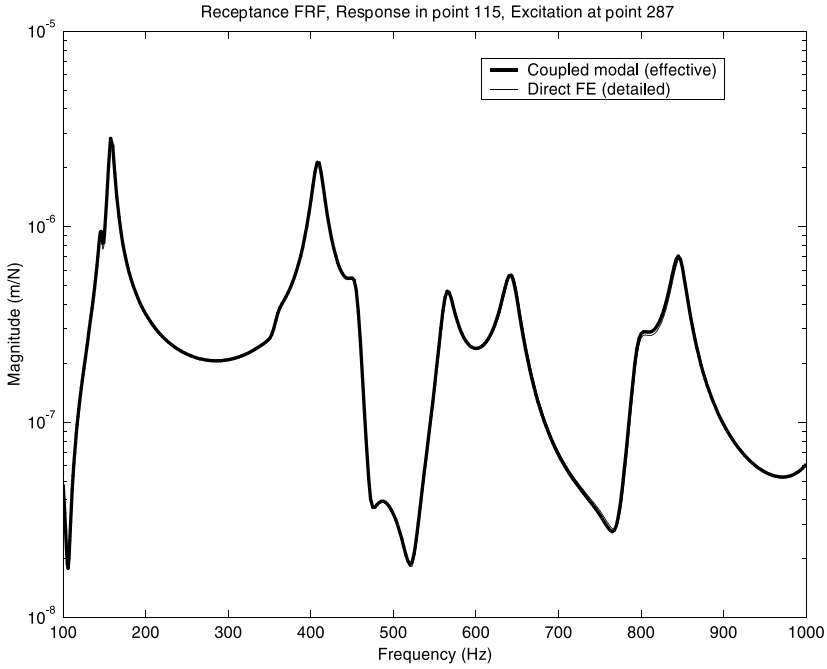

Fig. 6. Typical direct FE calculated (thin solid curve) transfer receptance FRF (response R_{33} in z-direction at point 115 and excitation in z-direction at point 287) for the laminate plate (with detailed modelling of the constituents) and corresponding effective coupled modal response model (thick solid curve), in the frequency interval 100–1000 Hz.

five frequency dependent damping functions. The material model is numerically tested on a symmetric composite laminate structure with dimensions 520 mm $\times$ 300 mm $\times$ 6 mm, by a combination of two aluminium plates and one Plexiglas plate.

Effective 3D homogeneous elastic (static) material constants were derived from known material data for each part of the composite laminate structure. A first-order approximation of effective elastic properties were performed according to the method proposed by Chen and Tsai (1996), for transverse stiffness properties, and using the classical laminated plate theory for in-plane properties, to account for the bending effect in the laminate. The effective in-plane elastic constants calculated by the classical laminated plate theory were found to converge to the values given by the method proposed by Chen and Tsai (1996) when the number of laminae increases.

The results from the elastic eigenvalue analysis of the proposed effective (homogenised) model, approximated by FE techniques, were found to be in good agreement with the corresponding detailed FE model for the first 20 modes, with a relative difference in eigenfrequency of less than 1.2%. The effective 3D transversely isotropic material model was found to be two times more accurate, in terms of predicted undamped eigenfrequencies, compared to classical laminated plate theory. It may also be seen that the degree of correlation between the detailed finite-element solution and the effective 3D model decreases, with increasing mode number. Differences in eigenfrequencies are expected as the actual deformation differs from the state of deformation assumed in the homogenisation procedure, the first order approximation to macro-mechanics.

Finally, forced vibration response calculations were made for the laminate structure using the 3D effective homogenised (dynamic) material models. The result, from comparisons with corresponding detailed

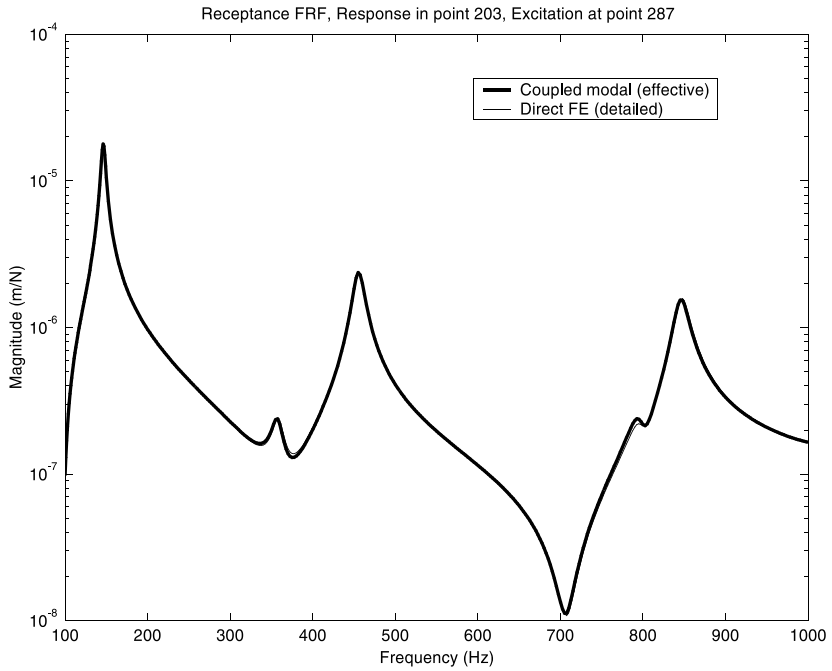

Fig. 7. Typical direct FE calculated (thin solid curve) transfer receptance FRF (response R_{33} in z-direction at point 203 and excitation in z-direction at point 287) for the laminate plate (with detailed modelling of the constituents) and corresponding effective coupled modal response model (thick solid curve), in the frequency interval 100–1000 Hz.

(layerwise) FE model, shows that the homogeneous laminate simulation of the test structure is very accurate in the studied frequency interval.

Acknowledgements

This work was performed under contract from the Swedish Defence Material Administration (contract no. 64914-LB114551). The funding provided is gratefully acknowledged. Many thanks also to my colleagues Krister Dovstam, Stella Einarsson, Peter Göransson, Robin Olsson, Niklas Sehlstedt, Ulf Tengzelius and Adam Zdunek for valuable discussions and criticism.

Appendix A. Definitions

The Cartesian matrix representations of the displacement field **u**, the symmetric stress field **T** and the (infinitesimal) strain tensor field **E** respectively are defined as:

$$\mathbf{u} = \mathbf{u}(\mathbf{x}, t) = [\, u_1 \quad u_2 \quad u_3 \,]^{\mathrm{T}}, \tag{A.1}$$

$$\mathbf{T} = [\, \sigma_{11} \quad \sigma_{22} \quad \sigma_{33} \quad \sigma_{12} \quad \sigma_{23} \quad \sigma_{31} \,]^{\mathrm{T}}, \tag{A.2}$$

$$\mathbf{E} = [\, \varepsilon_{11} \quad \varepsilon_{22} \quad \varepsilon_{33} \quad 2\varepsilon_{12} \quad 2\varepsilon_{23} \quad 2\varepsilon_{31} \,]^{\mathrm{T}}, \tag{A.3}$$

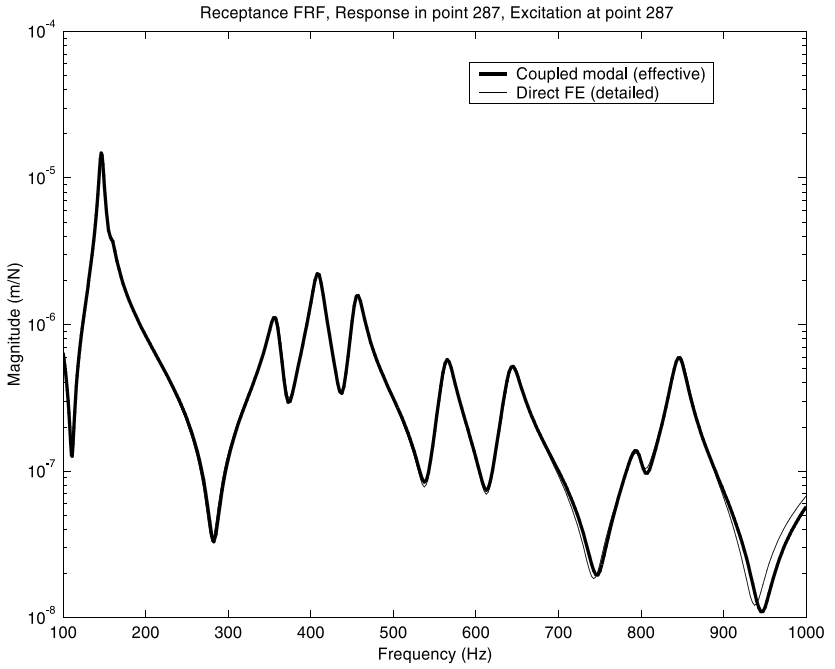

Fig. 8. Typical direct FE calculated (thin solid curve) transfer receptance FRF (response R_{33} in z-direction at point 287 and excitation in z-direction at point 287) for the laminate plate (with detailed modelling of the constituents) and corresponding effective coupled modal response model (thick solid curve), in the frequency interval 100–1000 Hz.

$$\varepsilon_{ik} = \frac{1}{2}\left\{ \frac{\partial u_i}{\partial x_k} + \frac{\partial u_k}{\partial x_i} \right\}, \tag{A.4}$$

where u_i, σ_{ik} and ε_{ik} are Cartesian vector and tensor components. The generalised transversely isotropic Hooke's law matrix, $\mathbf{H}$, is formally given by:

$$\mathbf{H} = \begin{bmatrix} H_{11} & H_{12} & H_{13} & 0 & 0 & 0 \\ & H_{11} & H_{13} & 0 & 0 & 0 \\ & & H_{33} & 0 & 0 & 0 \\ & & & (H_{11}-H_{12})/2 & 0 & 0 \\ & \text{SYM} & & & H_{66} & 0 \\ & & & & & H_{66} \end{bmatrix} \tag{A.5}$$

with a possible factorisation, $\mathbf{H} = H_{11}\mathbf{H}_{11} + H_{12}\mathbf{H}_{12} + H_{13}\mathbf{H}_{13} + H_{33}\mathbf{H}_{33} + H_{66}\mathbf{H}_{66}$, given by five matrices defined as:

$$\mathbf{H}_{11} = \frac{1}{2}\begin{bmatrix} 2 & 0 & 0 & 0 & 0 & 0 \\ & 2 & 0 & 0 & 0 & 0 \\ & & 0 & 0 & 0 & 0 \\ & & & 1 & 0 & 0 \\ & \text{SYM} & & & 0 & 0 \\ & & & & & 0 \end{bmatrix}, \tag{A.6}$$

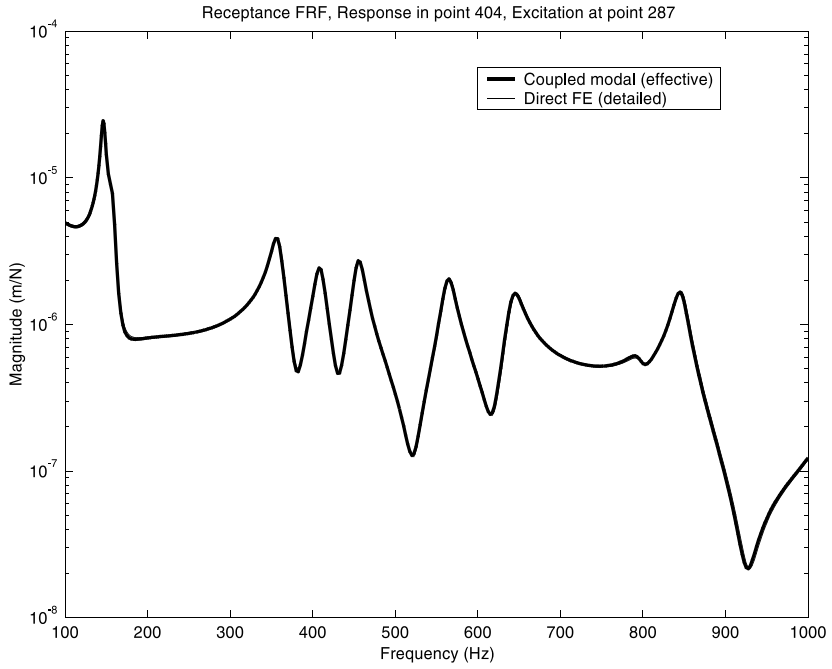

Fig. 9. Typical direct FE calculated (thin solid curve) transfer receptance FRF (response R_{33} in z-direction at point 404 and excitation in z-direction at point 287) for the laminate plate (with detailed modelling of the constituents) and corresponding effective coupled modal response model (thick solid curve), in the frequency interval 100–1000 Hz.

$$\mathbf{H}_{12} = \frac{1}{2}\begin{bmatrix} 0 & 2 & 0 & 0 & 0 & 0 \\ & 0 & 0 & 0 & 0 & 0 \\ & & 0 & 0 & 0 & 0 \\ & & & -1 & 0 & 0 \\ & \text{SYM} & & & 0 & 0 \\ & & & & & 0 \end{bmatrix} \tag{A.7}$$

$$\mathbf{H}_{13} = \begin{bmatrix} 0 & 0 & 1 & 0 & 0 & 0 \\ & 0 & 1 & 0 & 0 & 0 \\ & & 0 & 0 & 0 & 0 \\ & & & 0 & 0 & 0 \\ & \text{SYM} & & & 0 & 0 \\ & & & & & 0 \end{bmatrix}, \tag{A.8}$$

$$\mathbf{H}_{33} = \begin{bmatrix} 0 & 0 & 0 & 0 & 0 & 0 \\ & 0 & 0 & 0 & 0 & 0 \\ & & 1 & 0 & 0 & 0 \\ & & & 0 & 0 & 0 \\ & \text{SYM} & & & 0 & 0 \\ & & & & & 0 \end{bmatrix}, \tag{A.9}$$

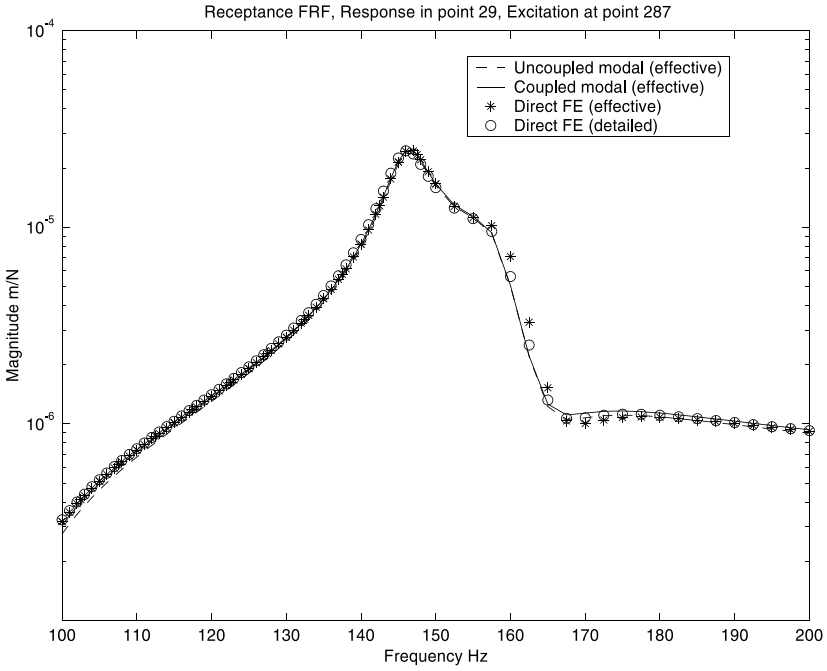

Fig. 10. Typical direct FE calculated ($\circ\circ\circ\circ$) transfer receptance FRF (response R_{33} in z-direction at point 29 and excitation in z-direction at point 287) for the laminate plate (with detailed modelling of the constituents). For comparisons the corresponding effective response models: direct FE ($****$), coupled modal (solid curve) and uncoupled modal (dashed curve), in the frequency interval 100–200 Hz.

$$\mathbf{H}_{66} = \begin{bmatrix} 0 & 0 & 0 & 0 & 0 & 0 \\ & 0 & 0 & 0 & 0 & 0 \\ & & 0 & 0 & 0 & 0 \\ & & & 0 & 0 & 0 \\ & \text{SYM} & & & 1 & 0 \\ & & & & & 1 \end{bmatrix} \tag{A.10}$$

and the corresponding compliance matrix $\mathbf{C}$ (cf. Eq. (A.5)):

$$\mathbf{C} = (\mathbf{H})^{-1} = \begin{bmatrix} C_{11} & C_{12} & C_{13} & 0 & 0 & 0 \\ & C_{11} & C_{13} & 0 & 0 & 0 \\ & & C_{33} & 0 & 0 & 0 \\ & & & 2(C_{11}-C_{12}) & 0 & 0 \\ & & \text{SYM} & & C_{66} & 0 \\ & & & & & C_{66} \end{bmatrix}. \tag{A.11}$$

Appendix B. AHL and generally coupled modes

The augmented Hook's law is (in the Laplace domain) given by Dovstam (1995):

$$\hat{\mathbf{H}}(\mathbf{x}, s) = \mathbf{H} + \sum_{l=1}^{N_a} \frac{s}{(\beta_l + s)} \mathbf{F}_l \mathbf{G}_l^{-1} \mathbf{F}_l, \tag{B.1}$$

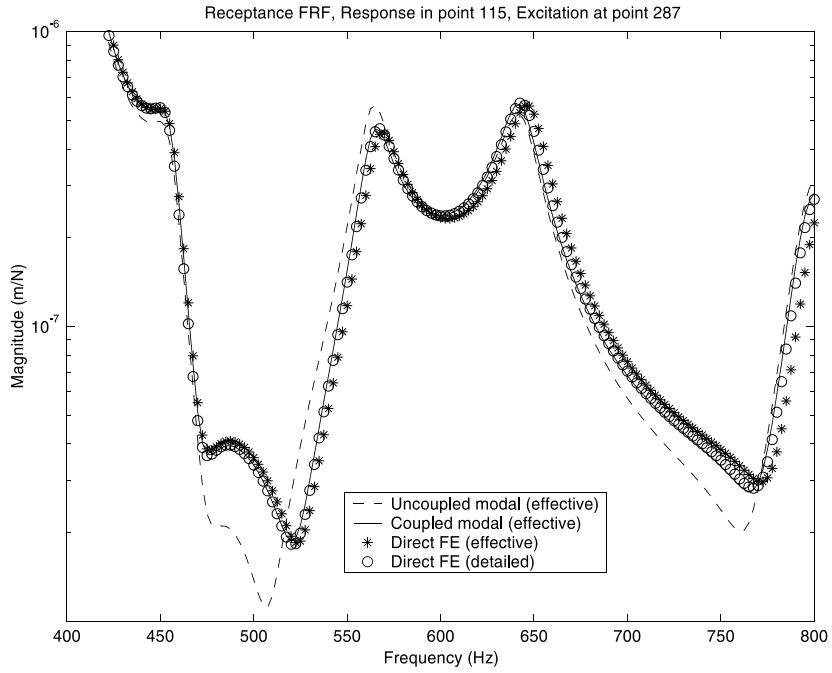

Fig. 11. Typical direct FE calculated ($\circ\circ\circ\circ$) transfer receptance FRF (response R_{33} in z-direction at point 115 and excitation in z-direction at point 287) for the laminate plate (with detailed modelling of the constituents). For comparisons the corresponding effective response models: direct FE ($*\,*\,*\,*$), coupled modal (solid curve) and uncoupled modal (dashed curve), in the frequency interval 400–800 Hz.

where $\mathbf{H}$ corresponds to the elastic part and where material damping, from N_a damping with processes relaxation frequencies β_l [1/s], is defined by real dissipation matrices $\mathbf{G}_l$ and real coupling matrices $\mathbf{F}_l$. For transversely isotropic material symmetry each coupling matrix is defined as:

$$\mathbf{F}_l = b_l \cdot \mathbf{H}_{11} + d_l \cdot \mathbf{H}_{12} + c_l \cdot \mathbf{H}_{13} + a_l \cdot \mathbf{H}_{33} + e_l \cdot \mathbf{H}_{66}, \tag{B.2}$$

where the material damping parameters are given by coefficients a_l, b_l, c_l, d_l and e_l. The matrices $\mathbf{H}_{11}$, $\mathbf{H}_{12}$, $\mathbf{H}_{13}$, $\mathbf{H}_{33}$ and $\mathbf{H}_{66}$ (defined in Appendix A) are associated with each independent, non-zero, modulus in the elastic part $\mathbf{H}$. The strength of the damping, in Eq. (B.1), is defined by:

$$\mathbf{F}_l \mathbf{G}_l^{-1} \mathbf{F}_l = a_{11}^{(l)} \cdot \mathbf{H}_{11} + a_{12}^{(l)} \cdot \mathbf{H}_{12} + a_{13}^{(l)} \cdot \mathbf{H}_{13} + a_{33}^{(l)} \cdot \mathbf{H}_{33} + a_{66}^{(l)} \cdot \mathbf{H}_{66}, \tag{B.3}$$

with normalised "process amplitudes" $A_{11}^{(l)}$, $A_{12}^{(l)}$, $A_{13}^{(l)}$, $A_{33}^{(l)}$ and $A_{66}^{(l)}$, defined as:

$$A_{11}^{(l)} = a_{11}^{(l)}/H_{11} = \left(b_l^2 + c_l^2 + d_l^2\right)/(H_{11}\alpha_l), \quad \left\{A_{11}^{(l)} \geqslant 0\right\} \in \mathbf{R}, \tag{B.4}$$

$$A_{12}^{(l)} = a_{12}^{(l)}/H_{12} = \left(2b_l d_l + c_l^2\right)/(H_{12}\alpha_l), \quad \left\{A_{12}^{(l)} \leqslant (H_{11}/H_{12})A_{11}^{(l)}\right\} \in \mathbf{R}, \tag{B.5}$$

$$A_{13}^{(l)} = a_{13}^{(l)}/H_{13} = c_l(a_l + b_l + d_l)/(H_{13}\alpha_l), \quad A_{13}^{(l)} \in \mathbf{R}, \tag{B.6}$$

$$A_{33}^{(l)} = a_{33}^{(l)}/H_{33} = \left(a_l^2 + 2c_l^2\right)/(H_{33}\alpha_l), \quad \left\{A_{33}^{(l)} \geqslant 0\right\} \in \mathbf{R}, \tag{B.7}$$

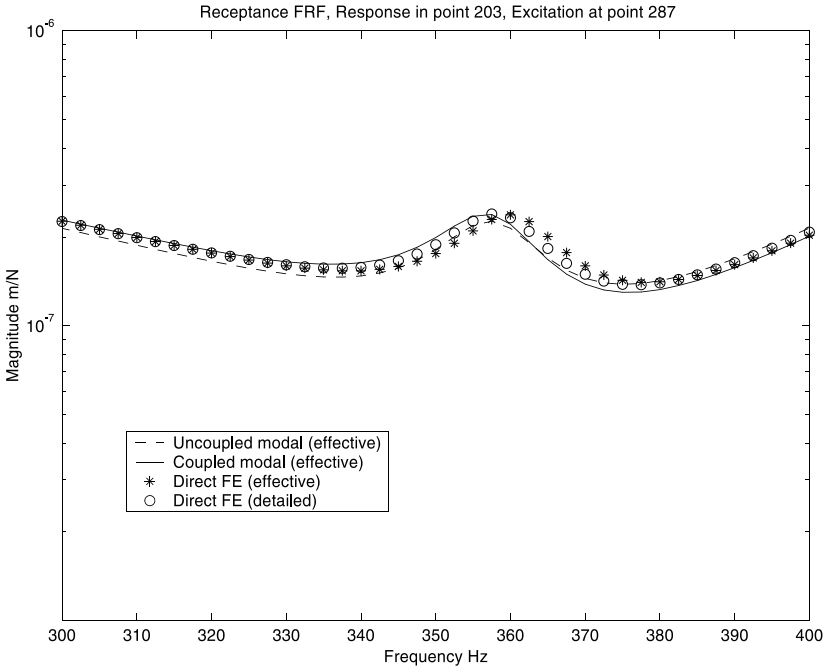

Fig. 12. Typical direct FE calculated ($\circ\circ\circ\circ$) transfer receptance FRF (response R_{33} in z-direction at point 203 and excitation in z-direction at point 287) for the laminate plate (with detailed modelling of the constituents). For comparisons the corresponding effective response models: direct FE ($*****$), coupled modal (solid curve) and uncoupled modal (dashed curve), in the frequency interval 300–400 Hz.

$$A_{66}^{(l)} = a_{66}^{(l)}/H_{66} = 2e_l^2/(H_{66}\alpha_l), \quad \left\{A_{66}^{(l)} \geqslant 0\right\} \in \mathbf{R}. \tag{B.8}$$

The generally coupled modal model (Dovstam, 1998, 2000b), is defined as:

$$a_m(\omega_m^2 + s^2)g_m(\tilde{\mathbf{T}}) + \frac{s^2}{\omega_m^2}\sum_{r=1}^{\infty}\left\langle \mathbf{H}\mathbf{C}_{\Delta}\mathbf{H}\mathbf{E}^{(m)}, \mathbf{E}^{(r)}\right\rangle g_r(\tilde{\mathbf{T}}) = \tilde{\boldsymbol{F}}_{\partial}^{(m)}, \tag{B.9}$$

where a_m denotes the modal mass, ω_m non-zero eigenfrequency, g_m modal stress coefficient (corresponding to the stress vector field $\tilde{\mathbf{T}}$), $\tilde{\boldsymbol{F}}_{\partial}^{(m)}$ modal force spectrum and $\mathbf{E}^{(m)}$ modal strain field number m. The relation $\left\langle \mathbf{H}\mathbf{C}_{\Delta}\mathbf{H}\mathbf{E}^{(m)}, \mathbf{E}^{(r)}\right\rangle$ is defined as a $\mathbf{L}_2^6(\Omega)$ inner product (cf. Dovstam, 2000b) where $\mathbf{C}_{\Delta}$ is the augmentation, corresponding to $\mathbf{H}$ and $\mathbf{H}_{\Delta}$, of the elastic compliance matrix $\mathbf{C}$. The matrix field $\mathbf{H}\mathbf{C}_{\Delta}\mathbf{H} = \lfloor \mathbf{H}\hat{\mathbf{H}}(\mathbf{x}, s)^{-1} - \mathbf{I}\rfloor\mathbf{H}$ is given, in terms of transversely isotropic material damping functions as:

$$\mathbf{H}\mathbf{C}_{\Delta}\mathbf{H} = b(s)H_{11}\mathbf{H}_{11} + d(s)H_{12}\mathbf{H}_{12} + c(s)H_{13}\mathbf{H}_{13} + a(s)H_{33}\mathbf{H}_{33} + e(s)H_{66}\mathbf{H}_{66}. \tag{B.10}$$

The relationship (B.9) may then be stated in matrix form:

$$\begin{bmatrix} B_{11} & B_{12} & B_{13} & B_{14} & \cdot & \cdot & \cdot \\ B_{21} & B_{22} & \cdot & \cdot & \cdot & \cdot & \cdot \\ \cdot & \cdot & \cdot & \cdot & \cdot & \cdot & \cdot \\ \cdot & \cdot & \cdot & B_{mr} & \cdot & \cdot & \cdot \\ \cdot & \cdot & \cdot & \cdot & \cdot & \cdot & \cdot \end{bmatrix} \begin{bmatrix} g_1(\tilde{\mathbf{T}}) \\ g_2(\tilde{\mathbf{T}}) \\ \cdot \\ g_r(\tilde{\mathbf{T}}) \\ \cdot \end{bmatrix} = \begin{bmatrix} \tilde{\boldsymbol{F}}_{\partial}^{(1)} \\ \tilde{\boldsymbol{F}}_{\partial}^{(2)} \\ \cdot \\ \tilde{\boldsymbol{F}}_{\partial}^{(m)} \\ \cdot \end{bmatrix}, \tag{B.11}$$

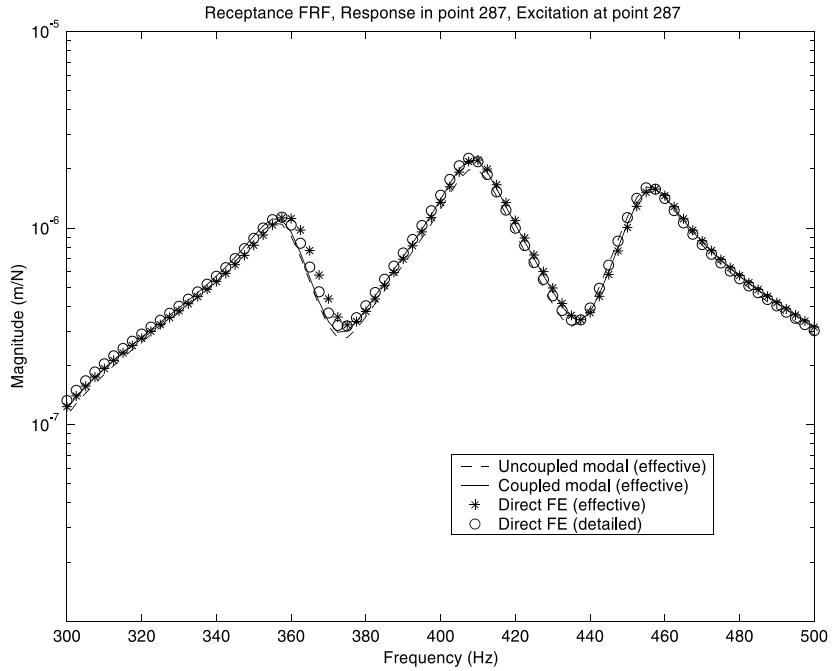

Fig. 13. Typical direct FE calculated ($\circ\circ\circ\circ$) transfer receptance FRF (response R_{33} in z-direction at point 287 and excitation in z-direction at point 287) for the laminate plate (with detailed modelling of the constituents). For comparisons the corresponding effective response models: direct FE ($*\,*\,*\,*$), coupled modal (solid curve) and uncoupled modal (dashed curve), in the frequency interval 300–500 Hz.

$$B_{mr} = \begin{cases} a_m\left[\omega_m^2 + s^2\left\{1 + \frac{1}{a_m\omega_m^2}\left\langle \mathbf{H}\mathbf{C}_{\Delta}\mathbf{H}\mathbf{E}^{(m)}, \mathbf{E}^{(m)}\right\rangle\right\}\right], & r = m, \\ \frac{s^2}{\omega_m^2}\left\langle \mathbf{H}\mathbf{C}_{\Delta}\mathbf{H}\mathbf{E}^{(m)}, \mathbf{E}^{(r)}\right\rangle, & r \neq m. \end{cases} \tag{B.12}$$

For non-zero frequencies the generalised Fourier coefficient $c_m(\tilde{\mathbf{u}})$ may be expressed in terms of the stress mode coefficients, $g_m(\tilde{\mathbf{T}})$:

$$c_m(\tilde{\mathbf{u}}) = \frac{\tilde{\boldsymbol{F}}_{\partial}^{(m)}}{a_m s^2} - \frac{\omega_m^2}{s^2} g_m(\tilde{\mathbf{T}}). \tag{B.13}$$

Appendix C. Approximation of effective three-dimensional elastic laminate properties

The effective in-plane engineering constants may then be approximated by the classical laminated plate theory, by using standard laminate compliance matrices:

$$\mathbf{A}' = (\mathbf{A})^{-1}, \tag{C.1}$$

$$v_{21} = -\frac{A'_{12}}{A'_{11}}, \tag{C.2}$$

$$\mathbf{D}' = (\mathbf{D})^{-1}, \tag{C.3}$$

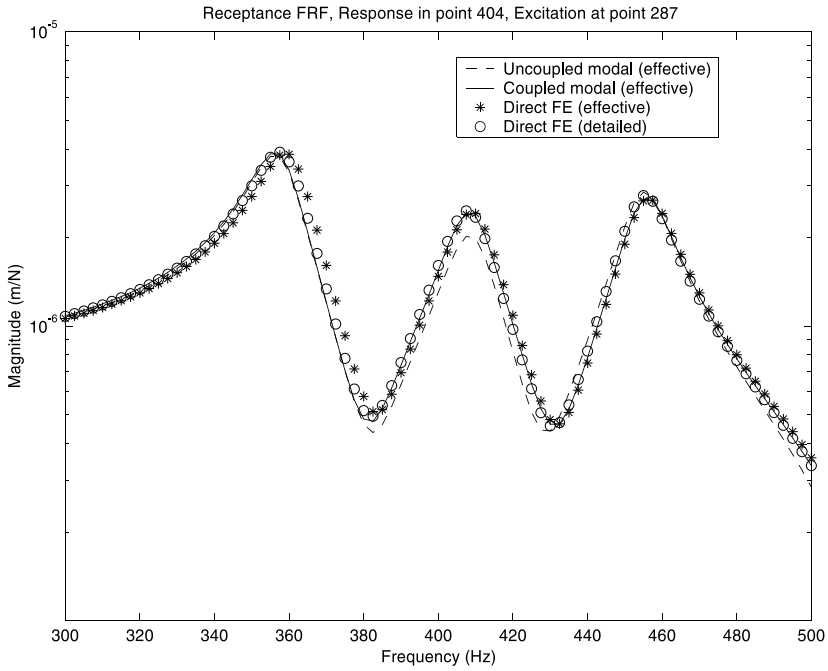

Fig. 14. Typical direct FE calculated ($\circ\circ\circ\circ$) transfer receptance FRF (response R_{33} in z-direction at point 404 and excitation in z-direction at point 287) for the laminate plate (with detailed modelling of the constituents). For comparisons the corresponding effective response models: direct FE ($****$), coupled modal (solid curve) and uncoupled modal (dashed curve), in the frequency interval 300–500 Hz.

$$E_1 = \frac{12}{h^3 D'_{11}}, \tag{C.4}$$

$$G_{12} = \frac{E_1}{2(1+v_{21})}, \tag{C.5}$$

where v_{21} denotes the in-plane poisson's ratio, G_{12} the shear modulus, E_1 the in-plane flexural modulus and h is the total laminate thickness. The matrix **A**, with components A_{ij} $(i,j=1,2,3)$, denotes the laminate extension stiffness matrix and **D**, with components D_{ij} $(i,j=1,2,3)$, denotes the laminate bending stiffness matrix. The coupling between the bending stiffness and extension stiffness is given by the coupling stiffness matrix **B**, B_{ij} $(i,j=1,2,3)$. In the case of symmetric laminates all components are zero $B_{ij}=0$.

Remaining, effective (out-of-plane) material properties are calculated by adopting a 3D (first-order) method, proposed by Chen and Tsai (1996), assuming that the distributions of in-plane strains and interlaminar stresses are constant. The effective material elasticities are formally given by:

$$H_{33} = \left(\sum_{k=1}^{N} \frac{t_k}{H_{33}^{(k)}} \right)^{-1}, \tag{C.6}$$

$$H_{13} = H_{33} \sum_{k=1}^{N} t_k \frac{H_{13}^{(k)}}{H_{33}^{(k)}}, \tag{C.7}$$

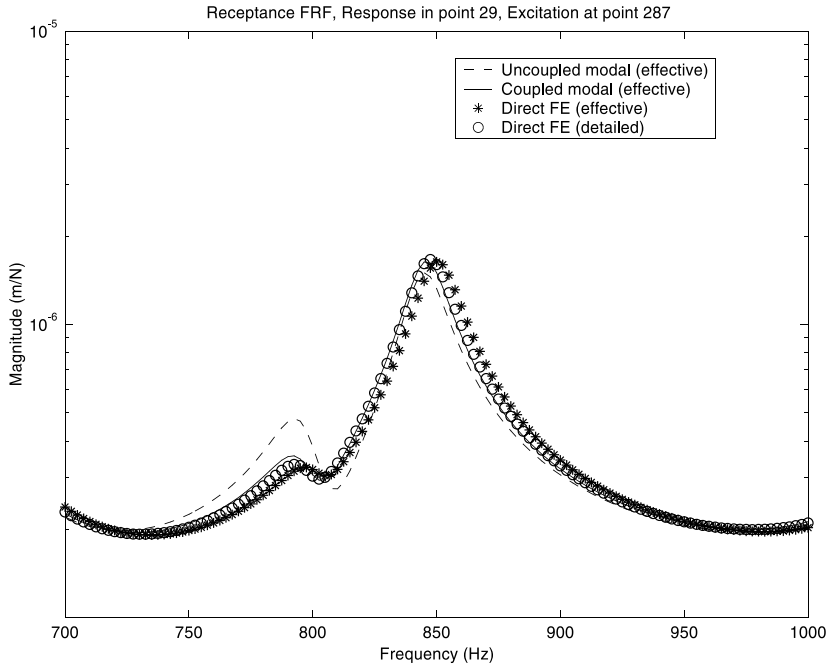

Fig. 15. Typical direct FE calculated ($\circ\circ\circ\circ$) transfer receptance FRF (response R_{33} in z-direction at point 29 and excitation in z-direction at point 287) for the laminate plate (with detailed modelling of the constituents). For comparisons the corresponding effective response models: direct FE ($****$), coupled modal (solid curve) and uncoupled modal (dashed curve), in the frequency interval 700–1000 Hz.

$$C_{ij} = \sum_{k=1}^{N} t_k C_{ij}^{(k)}, \quad i,j = 5,6 \tag{C.8}$$

$$\begin{bmatrix} H_{55}^{(k)} & H_{56}^{(k)} \\ H_{65}^{(k)} & H_{66}^{(k)} \end{bmatrix} = \begin{bmatrix} C_{55}^{(k)} & C_{56}^{(k)} \\ C_{65}^{(k)} & C_{66}^{(k)} \end{bmatrix}^{-1}, \tag{C.9}$$

where $t_k = |z_{k-1} - z_k|/h$, $(k = 1,2,\ldots,N)$, is the volume fraction of the kth lamina, with each lamina stiffness component k transformed from the local material symmetry reference system, given by the transformation matrix $\mathbf{Q}$, $\mathbf{H}^{(k)} = \mathbf{Q}\overline{\mathbf{H}}^{(k)}$ (cf. Christensen, 1979), to the global laminate reference system. Note that the compliance matrix, Eq. (C.12), components C_{56} and C_{65} are both zero in the case of transversely isotropic material symmetry.

The effective (out-of-plane) elastic engineering material constants may then be calculated using the Eqs. (4)–(9) and (C.1)–(C.9):

$$E_3 = \frac{E_1}{(4 - E_1/G_{12})(H_{13}/H_{33})^2 + E_1/H_{33}}, \tag{C.10}$$

$$\nu_{31} = \frac{H_{13}}{2\kappa_{21}}, \tag{C.11}$$

$$\kappa_{21} = \frac{H_{13}^2}{(H_{33} - E_{33})}, \tag{C.12}$$

$$G_{31} = H_{66}, \tag{C.13}$$

where these material parameters are related to the transverse stress and strain with the corresponding engineering constants given by the elastic transverse moduli E_3, Poisson's ratio v_{31} ($v_{31} = v_{32}$) and the shear modulus G_{31} ($G_{31} = G_{23}$).

References

Bagley, R.L., Torvik, P.J., 1983. Fractional calculus – a different approach to the analysis of viscoelastically damped structures. AIAA J. 21, 741–748.

Barbero, E.J., Luciano, R., 1995. Micromechanical formulas for the relaxation tensor of linear viscoelastic composites with transversely isotropic fibres. Int. J. Solids Struct. 32(13), 1859–1872.

Barrett, D.J., 1992. An anisotropic laminated damped plate theory. J. Sound Vib. 154(3), 453–465.

Carrera, E., 2000. An assessment of mixed and classical theories on global and local response of multilayered orthotropic plates. Compos. Struct. 50, 183–198.

Chandra, R., Singh, S.P., Gupta, K., 1999. Damping studies in fiber-reinforced composites – a review. Compos. Struct. 46, 41–51.

Chang, S., 1986. Effective moduli of composite materials in dynamic problems. AIAA J. 25(3), 464–469.

Christensen, R.M., 1979. Mechanics of composite materials. Wiley, New York, ISBN 0-89464-501-3.

Chen, H., Tsai, S.W., 1996. Three-dimensional effective elastic constants for thick laminates. J. Compos. Mater. 30(8), 906–917.

Chou, P.C., Carleone, J., 1972. Elastic constants of layered media. J. Compos. Mater. 6, 80–93.

Dalenbring, M., 1999. Damping function estimation based on measured vibration frequency responses and finite-element displacement modes. Mech. Syst. Signal Process. 13(4), 547–569.

Dalenbring, M., 2001a. Validation of estimated isotropic material damping properties and vibration response prediction. J. Sound Vib., submitted for publication.

Dalenbring, M., 2001b. Experimental material damping estimation for transversely isotropic laminate structures. Int. J. Solids Struct., submitted for publication.

Dovstam, K., Dalenbring, M., 1997. Damping function estimation based on modal receptance models and neural nets. Res. J. Comput. Mech. 19, 271–286.

Dovstam, K., 1995. Augmented Hooke's law in frequency domain. A three dimensional, material damping formulation.. Int. J. Solids Struct. 32, 2835–2852.

Dovstam, K., 1997. Receptance model based on isotropic damping functions and elastic displacement modes. Int. J. Solids Struct. 34, 2733–2754.

Dovstam, K., 1998. On material damping modelling and modal analysis in structural dynamics. Doctoral Thesis. Department of Solid Mechanics, Royal Institute of Technology, Stockholm.

Dovstam, K., 2000a. Augmented Hooke's law based on alternative stress relaxation models. Res. J. Comput. Mech. 26, 90–103.

Dovstam, K., 2000b. Simulation of damped vibrations based on augmented Hooke's law and elastic modes of vibration. Int. J. Solids Struct. 37, 5413–5445.

Einarsson, S., Dalenbring, M., 2000. The effect of uncertainty in static moduli on extracted damping from dynamic response of highly damped systems. Res. J. Comput. Mech., submitted for publication.

Ernie, R.B., Rizzo, R.R., 1970. Three-dimensional laminate moduli. Res. J. Compos. Mater. 4, 150–154.

Ewins, D.J., 1986. Modal Testing: Theory and Practice. Research Studies Press Ltd. and Brel & Kjaer. Letchworth, Hertfordshire, England.

Finegan, I.C., Gibson, R.F., 1999. Recent research on enhancement of damping in polymer Composites. Compos. Struct. 44, 89–98.

Gibson, R.F., 1990. Dynamic mechanical properties of advanced composite materials and structures: a review of recent research. Shock Vib. Digest 22 (8), 3–12.

Gibson, R.F., 1994. Principles of composite material mechanics. McGraw-Hill, New York, ISBN 0-07-023451-5.

Göransson, P., 1988. ASKA Acoustics. Theory and applications. FFA TN 1988(13). Aeronautical Research Institute of Sweden, Stockholm.

Hashin, Z., 1970. Complex moduli of viscoelastic composites-I. General theory and application to particulate composites. Int. J. Solids Struct. 6, 539–552.

Hyer, M.W., 1998. Stress analysis of fiber-reinforced composite materials. WCB McGraw-Hill, Singapore, ISBN 0-07-115983-5.

Hwang, S.J., Gibson, R.F., 1992a. The use of strain energy-based finite element techniques in the analysis of various aspects of damping of composite materials and structures. J. Compos. Mater. 26 (17), 2585–2605.
Hwang, S.J., Gibson, R.F., 1992b. Contribution of interlaminar stresses to damping in thick laminated composites under uniaxial extension. Compos. Struct. 20, 29–35.
Hwang, S.J., Gibson, R.F., Singh, J., 1992. Decomposition of coupling effects on damping of laminated composite under flexural vibration. Compos. Sci. Technol. 43, 159–169.
Hwang, S.J., Gibson, R.F., 1991. The effect of three-dimensional states of stress on damping of laminated composites. Compos. Sci. Technol. 41, 379–393.
Johnson, C.D., Kienholz, D.A., 1982. Finite element prediction of damping in structures with constrained viscoelastic layers. AIAA J. 20 (9), 1284–1290.
Kant, T., Swaminathan, K., 2000. Estimation of transverse/interlaminar stresses in laminated composites – a selective review and survey of current developments. Compos. Struct. 49, 65–75.
Khdeir, A.A., Reddy, J.N., 1999. Free vibrations of laminated composite plates using second-order shear deformation theory. Comput. Struct. 71, 617–626.
Koo, K.N., Lee, I., 1995. A refined analysis of vibration and damping for anisotropic laminate in cylindrical bending. J. Sound Vib. 184 (4), 553–566.
Korjakin, A., Rikards, R., Chate, A., Altenbach, H., 1998. Analysis of free damped vibrations of laminated composite conical shells. Compos. Struct. 41, 39–47.
Lesieutre, G.A., Bianchini, E., 1995. Time domain modeling of linear viscoelasticity using anelastic displacement fields. Trans. ASME 117, 424–430.
Maher, A., 1994. Evaluative eigen analysis of composite structures. Compos. Struct. 29, 191–195.
Maher, A., Ramadan, F., Gupta, K., 1999a. Modeling of vibration damping in composite structures. Compos. Struct. 46, 163–170.
Maher, A., Ramadan, F., Ferra, M., 1999b. Modeling of vibration damping in composite structures. Compos. Struct. 46, 163–170.
Pagano, N.J., 1974. Mechanics of composite materials. In: Sendeckyj, G.P. (Ed.), Composite Materials, vol. 2. Academic Press, New York.
Pagano, N.J., 1969. Exact solutions for composite laminates in cylindrical bending. J. Compos. Mater. 3, 398–411.
Pagano, N.J., 1970. Exact solutions for rectangular bidirectional composites and sandwich plates. J. Compos. Mater. 4, 20–34.
Pipes, R.B., Pagano, N.J., 1970. Interlaminar stresses in composite laminates under uniform axial extension. J. Compos. Mater. 4, 538–548.
Postma, G.W., 1955. Wave propagation in a stratified medium. Geophysics 20 (4), 780–806.
Reddy, J.N., Phan, N.D., 1985. Stability and vibration of isotropic, orthotropic and laminated plates according to a higher-order shear deformation theory. J. Sound Vib. 98 (2), 157–170.
Reddy, J.N., 1997. Mechanics of laminated composite plates, theory and analysis. CRC Press, Florida, ISBN 0-8493-3101-3.
Rikards, R., Chate, A., Barkanov, E., 1993. Finite element analysis of damping the vibrations of laminated composites. Comput. Struct. 47 (6), 1005–1015.
Rikards, A., Chate, A., Bledzki, K., Kushnevsky, V., 1994. Numerical modelling of damping properties of laminated composites. Mech. Compos. Mater. 30 (3), 256–266.
Roy, A.K., Tsai, S.W., 1992. Three-dimensional effective moduli of orthotropic and symmetric laminates. J Appl. Mech. 59, 39–47.
Rytov, S.M., 1956. Acoustical properties of a thinly laminated medium. Akust. Zh. 2, 71 [Sov. Phys. Acoust. 2, 68, 1956].
Sun, C.T., Li, S., 1988. Three-dimensional effective elastic constants for thick laminates. J. Compos. Mater. 22, 629–639.
Sun, C.T., Lu, Y.P., 1995. Vibration damping of structural elements. Prentice Hall PTR, Englewood Cliffs, New Jersey.
Sun, C.T., Lou, J., McCoy, R.W., 1996. Analysis of wave propagation in thick laminates using effective moduli. Compos. Part B 27B, 613–621.
Saravanos, D.A., Chamis, C.C., 1991. Computational simulations of damping in composite structures. J. Reinf. Plast. Compos. 10, 256–278.
Saravanos, D.A., 1994. Integrated damping mechanics for thick composite laminates and plates. J. Appl. Mech. 61, 375–383.
Saravanos, D.A., Pereira, J.M., 1995. Dynamic characteristics of specially composite structures with embedded damping layers. Trans. ASME 117, 62–69.
Ungar, E.E., Kerwin Jr., E.M., 1962. Loss Factors of Viscoelastic systems in terms of energy concepts. J. Acoust. Soc. Am. 34, 954–957.
Whitcomb, J., Noh, J., 2000. Concise derivation of formulas for 3D sublaminate homogenization. J. Compos. Mater. 34 (6), 522–535.
Yarlagadda, S., Lesieutre, G., 1995. Fiber contribution to modal damping of polymer matrix composite panels. J. Spacecraft Rockets 32 (5), 825–831.